Journal of Power Sources 373 (2018) 172–183

Contents lists available at ScienceDirect

Journal of Power Sources

journal homepage: www.elsevier.com/locate/jpowsour

Lithium ion batteries (NMC/graphite) cycling at 80 °C: Different electrolytes and related degradation mechanism

R. Genieser[a,*], S. Ferrari[a], M. Loveridge[a], S.D. Beattie[b], R. Beanland[c], H. Amari[c], G. West[a], R. Bhagat[a]

[a] WMG, University of Warwick, Coventry, CV4 7AL, UK
[b] BTInnovations, St. Croix, Nova Scotia, B0N 2E0, Canada
[c] Department of Physics, University of Warwick, Coventry, CV4 7AL, UK

HIGHLIGHTS

- Additives prevent initial solvent oxidation but not resistance increase of cathode.
- Surface reconstruction layer of cathode did not grow past high temperature cycling.
- New resistance layers between primary grains due to particle cracking.

GRAPHICAL ABSTRACT

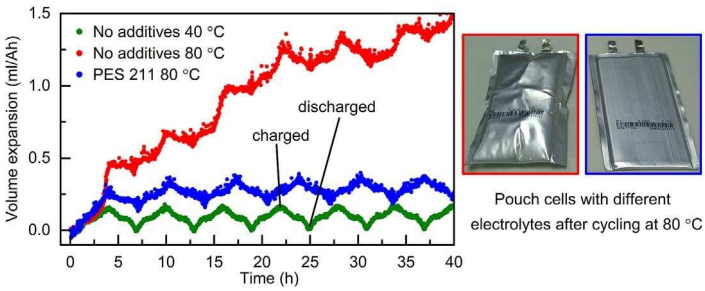

ARTICLE INFO

Keywords:
Li-ion battery
Elevated temperature
Electrolyte additives
Electrode degradation
Cell swelling

ABSTRACT

A comprehensive study on high temperature cycling (80 °C) of industrial manufactured Li-ion pouch cells (NMC-111/Graphite) filled with different electrolytes is introduced. Ageing processes such as capacity fade, resistance increase and gas generation are reduced by the choice of appropriate electrolyte formulations. However, even by using additive formulations designed for elevated temperatures a large resistance increase is observed after 200 cycles and more (which does not happen at 55 °C). Symmetrical EIS (Electrochemical Impedance Spectroscopy) shows that the cathodic charge transfer resistance is the main reason for this behaviour. Nonetheless most of the active Li is still available when cycling with suitable additives. No change of the cathode crystalline structure or a growth of the cathodic surface reconstruction layer is observed post cycling at 80 °C. Therefore a disintegration of NMC secondary particles is believed to be the main reason of the cell failure. A separation of single grains is leading to new decomposition and reconstruction layers between primary particles and an increased charge transfer resistance. Further approaches to improve the high temperature cycle stability of NMC based materials should therefore be aimed at the cathode particles morphology in combination with similar electrolyte formulations as used in this study.

1. Introduction

Manufacturers of Li-ion batteries specify the upper operational temperature range of their products to be approximately 50–60 °C. If operated at higher temperatures than suggested, cells have been shown to generate gas and age much faster [1–3]. However, some industrial applications require their devices to be thermally stable up to 80 °C. Such applications include cells for sensor technologies, military

* Corresponding author.
E-mail addresses: R.Genieser@warwick.ac.uk, R.Genieser@gmx.net (R. Genieser).

https://doi.org/10.1016/j.jpowsour.2017.11.014
Received 13 August 2017; Received in revised form 20 September 2017; Accepted 4 November 2017

operations and downhole, high temperature environments (such as mining or oil and gas exploration) [1]. More common situations such as prolonged sunlight exposure on the dashboard of a car, can also result in temperature environments ≥75 °C [4]. Batteries containing $Li(Ni_{1/3}Mn_{1/3}Co_{1/3})O_2$ (NMC-111) as a cathode material have been reported to show an increased thermal stability compared to cells based on $LiCoO_2$ (LCO) or $Li(Ni_{0.8}Co_{0.15}Al_{0.05})O_2$ (NCA) [5–8]. During thermal runaway tests a delayed temperature onset was observed with minor amounts of energy released. A similar observation has been reported for cells based on $LiFePO_4$ (LFP) cathodes or $Li_4Ti_5O_{12}$ (LTO) anodes [7,9,10]. However, the use of either of these materials results in lower cell voltages and worse cycling stabilities at elevated temperatures [3,11–13]. Several publications have focused on the thermal stability of Li-ion batteries at temperatures above 80 °C and higher, yet little information has been reported around investing the degradation of cells cycling under these conditions [5–7,14–17]. In a half-cell study Andersson and Edström found that the morphology and chemical composition of the solid electrolyte interface (SEI) formed on graphite anodes changed during cycling at 80 °C [18]. Lithium alkyl carbonates disappeared and LiF crystals were found to cover the surface. The degradation of the cathode material has been the focus of many studies, stating that a gain in electrode resistance of layered materials such as LCO leads to an increased capacity fade [1,19,20]. Recent publications show the importance of studying full cells for a broader understanding of degradation mechanisms, as it is believed that both electrodes can interact with each other [21–24]. Another potentially misleading observation from half-cells vs. lithium can be seen for the work published by Chang et al. [25]. An improvement in capacity retention at elevated temperatures was achieved by Ti and Fe coatings of LFP cathodes. However, when cycling the same electrodes vs. carbon anodes an adverse effect was discovered. Many other types of coatings have been applied to positive and negative electrode materials to improve the cycling stability at high temperatures [26–29]. These will not be comprehensively explored within the scope of this article. NCA, due to its high specific capacity, has been studied frequently at elevated temperatures using full cells. Sasaki and Muto et al. showed a moderate capacity retention in cylindrical cells with this cathode type at 80 °C [30,31]. After 350 cycles, approximately 80% of the capacity was still available. They found that the capacity fade directly correlated with the amount of inactive Ni^{+2} and Ni^{+3} areas. Both, Kojima and Muto et al. analysed NCA full cells aged at 70 and 80 °C [31,32]. They found that in addition to a phase reconstruction layer, large quantities of fluoride species were located between grain boundaries of primary particles. Recently the interest in layered $Li(Ni_{1-x-y}Mn_xCo_y)O_2$ as a positive electrode material has increased. This is linked to its advanced thermal stability compared with NCA in combination with a high specific capacity and an acceptable cycle stability [8]. These characteristics are related to large quantities of Mn^{4+}-ions, which stabilize the cathode structure at high state of charges (SoC) [33,34]. Bang et al. also found that the stability of these materials improves with higher Mn contents and the capacity increases with larger Ni contents within the structure [35]. This is because the redox reaction $Ni^{2+} \leftrightarrow Ni^{4+}$ primarily compensates for the charge transfer during lithiation and delithiation [34]. Bodenes et al. cycled $Li(Ni_{1-x-y}Mn_xCo_y)O_2$ vs. graphite in cylindrical cells at elevated temperatures and analysed the aged electrodes via X-ray photoelectron spectroscopy (XPS) [36,37]. In contrast to results based on NCA, they concluded that the resistance increase observed for cycling cells at 85 °C might be a result of the growing anode SEI. When cycled at 120 °C they found a migration of the PVDF binder to the cathode surface, resulting in an even faster capacity fade and resistance increase. Many of the above mentioned studies are focused on the degradation of the electrode materials. There has been minimal information given about the possible influence of electrolyte compositions used for these experiments. Most published work concerning different electrolyte formulations has been performed either on coin cell levels (half-cells vs. Li/Li^+) or at lower temperatures (≤60 °C). Xu et al. found that 2% of propane sultone as an additive influenced the composition of the cathode decomposition layer [38]. This resulted in a better cycle stability of coin cells following storage at 75 °C. Xia et al. used various similar substances based on sulphites, sulphates, sultones, di-sulfonates and also the well-known vinylene carbonate (VC) [39]. They cycled NMC(111)/graphite pouch cells with various mixtures of different additives at 55 °C. A combination of these substances led to improved cycling stabilities compared with single component additions. It was suggested that different additives can interact with each other but to our knowledge no mechanism was proposed which would substantiate these findings. In this study, our objective is to determine the influence of different electrolyte compositions on the cycling performance of $Li(Ni_{1/3}Mn_{1/3}Co_{1/3})O_2$/graphite pouch cells cycled at 80 °C. Additionally to study values like resistance increase, capacity fade and volume expansion also the degradation state of single cell components was evaluated. We thereby used post-mortem analyses such as symmetrical EIS measurements, surface-sensitive techniques (XPS), bulk structural measurements (XRD) and TEM/STEM.

2. Experimental

2.1. Cell filling, formation and cycling

$Li[Ni_{1/3}Mn_{1/3}Co_{1/3}]O_2$ (NMC111)/graphite pouch cells (ca. 1.2 Ah) without electrolyte were obtained from LiFun Technology (Xinma Industry Zone, Golden Dragon Road, Tianyuan District, Zhuzhou City, Hunan Province, PRC, 412000, China). The electrode loading for the anode was 95 g/m² with 95% active material, 3.8% binder (CMC/SBR) and 1.2% conductive carbon. The cathode loading was 185 g/m² with 96.4% active material, 2% binder and 1.6% conductive carbon. Cells arrived vacuum sealed with extra pouch material for the degassing process still attached. Before filling with electrolyte, the cells were cut open within the excess pouch foil region and dried at 70 °C, under vacuum for at least 12 h, to remove most residual water. Afterwards each cell was filled in a dry room (dew point of -45 °C) with 4.8 g of electrolyte (4 g Ah-1). The electrolyte compositions and their suppliers can be found in Table 1.

Composition C was achieved by adding PES (Prop-1-ene-1,3-sultone – Fluorochem, 95%), DTD (1,5,2,4-Dioxa-dithiane 2,2,4,4-tetraoxide – Fluorochem, 95%) and TTSPi (Tris-trimethylsilyl-phosphite – Sigma Aldrich, 95%) to Electrolyte A. Electrolytes A, B and E exhibited a water content around 2 ppm, while the modified electrolyte C measured approximately 20 ppm (due to the water within the additives). Cells with electrolyte D were pre-filled by the manufacturer and so an analysis of the water content was not possible. After filling, the cells were transferred into a vacuum sealer (MFC-2 Solith) and underwent a soak cycle between 100 and 800 mbar before being sealed at a final pressure of 10 mbar. For the formation cycle, all cells were held for 24 h at 1.5 V in a climate chamber set at 40 °C and charged at 60 mA (C/20) to 3.8 V. A VMP3 potentiostat (Bio-Logic) was used for all electrochemical cycling. After the initial formation the cells were cut open in the dry room and resealed under vacuum (degassing step). Before cycling at elevated

Table 1
Electrolyte compositions for cells cycled at 80 °C – the salt concentration for each composition was 1 M $LiPF_6$ except for electrolyte E where it was 1.2 M $LiPF_6$.

No.	Solvents (vol. Ratio)	Additives (mass ratio)	Supplier	Colour Code
A	EC:EMC (3:7)	none	BASF (LP57)	Orange
B	EC:EMC (3:7)	1% VC	Soulbrain	Red
C	EC:EMC (3:7)	2% PES, 1% DTD, 1% TTSPi	Electrolyte A modified	Green
D	EC:PC:DEC (35:30:45)	1% VC, 1% PES + other	LiFun Technology	Blue
E	EC:EMC (1:3)	15% FEC, 3% VC	Soulbrain	Purple

temperatures the formation step was completed at 25 °C and the cells also underwent two comparison cycles at 240 mA (C/5) to demonstrate reproducible capacity and resistance values. For long-term cycling at least three cells of each electrolyte composition were placed in thermal chambers set at 80 °C (± 0.1 °C) and were cycled between 2.5 V and 4.2 V in a CC-CV mode with 400 mA (C/3) constant current (CC) down to 60 mA (C/20) during the constant voltage step (CV) at 4.2 V. Every 25 cycles the impedances of the pouch cells were measured after a discharge to 3.5 V with 30 min waiting time, using potentiostatic electrochemical impedance spectroscopy (PEIS). The scanning range was between 100 kHz and 10 mHz with an amplitude of 10 mV. Fig. S1a shows a typical Nyquist plot for EIS data of these pouch cells, measured at room temperature and at 80 °C. The data were fitted by using ZView with the following circuit elements: inductor (L), series resistance (R_s), SEI resistance (R_{sei}), charge transfer resistance (R_{ct}), constant phase elements (CPE) and Warburg element (W). Fig. S1b shows the circuit model used for curve fittings at 25 °C. Due to faster kinetics at elevated temperatures, only one semicircle was observed and this effect continued as a function of cycle number. The circuit was therefore simplified by combining the SEI and charge transfer resistance for further evaluations (shown as R_{ct} within the results). The experimental setup for the in-situ expansion measurements has been described in detail by Aiken et al. [40]. Thin film load cells (0.2 N) were obtained from Strain Measurement Devices and the voltage reading was amplified using a self-built device. The signal was measured via the external VMP3 port to enable time resolved data acquisition of battery voltage and volume expansion.

2.2. Post mortem analyses

After the cycling procedure at 80 °C each cell was discharged at 25 °C to 3.5 V and the impedance was re-measured. The batteries were opened in an argon filled glovebox (O_2 and H_2O below 0.1 ppm) and the electrodes were washed with DMC (di-methyl carbonate) for further use. SEM images were obtained using a Carl Zeiss Sigma Field Emission Scanning Electron Microscope (FE-SEM) at 5 kV accelerating voltage in combination with in-lens detection at working distances of approximately 2 mm. Coin sized discs (15 mm diameter) of anodes and cathodes were cut from the aged electrodes to build coin cells inside the glovebox. Symmetrical cells (two discs of the same electrode against each other) were assembled according to Petibon et al. and half-cells were built against lithium (15.6 mm discs – PI-KEM) [41]. All cells were filled with fresh electrolyte of composition A (Table 1). The impedance for symmetrical coin cells was measured at 25 °C using the same settings as for the pouch cell measurements. Half cells have been cycled with a MACCOR Series 4000 system using different current densities. X-ray photoelectron spectroscopy (XPS) was carried out using a Kratos AXis Ultra DLD spectrometer (Kratos Analytical Ltd.) with monochromatic Al-Kα source (hn = 1486.6 eV). High-resolution spectra were obtained using a 20 eV pass energy and an analysis area of approximately 300 × 700 μm. Samples were transferred under argon atmosphere and peak fitting was conducted by using the CasaXPS software. X-ray crystallography (XRD) was performed using a PANalytical X'Pert³ MRD diffractometer with a Cu $K\alpha_1$ radiation operated at 45 kV and 40 mA. Data were collected at a 2θ range of 15–70° at 1°/min. Lattice parameters were calculated by Rietveld refinement using TOPAS. Scanning Transmission Electron Microscopy (STEM) samples and SEM cross-sections were prepared using a FEI Scios dual beam scanning electron/focused ion beam microscope (SEM/FIB) at 30 kV and changing currents (3 nA milling down to 0.1 nA for surface cleaning). Samples were baked under vacuum at 50 °C for at least 12 h before transferring them into a JEOL ARM 200F. The microscope was operated at 200 kV in STEM mode and images were acquired with an annular dark-field (ADF) detector. EELS spectra were obtained, using a GatanQuantum-SE spectrometer with 0.25 eV per channel dispersion. The full width at half maximum (FWHM) of the zero-loss peak (ZLP) was 2 eV with a center error of 0.05 eV.

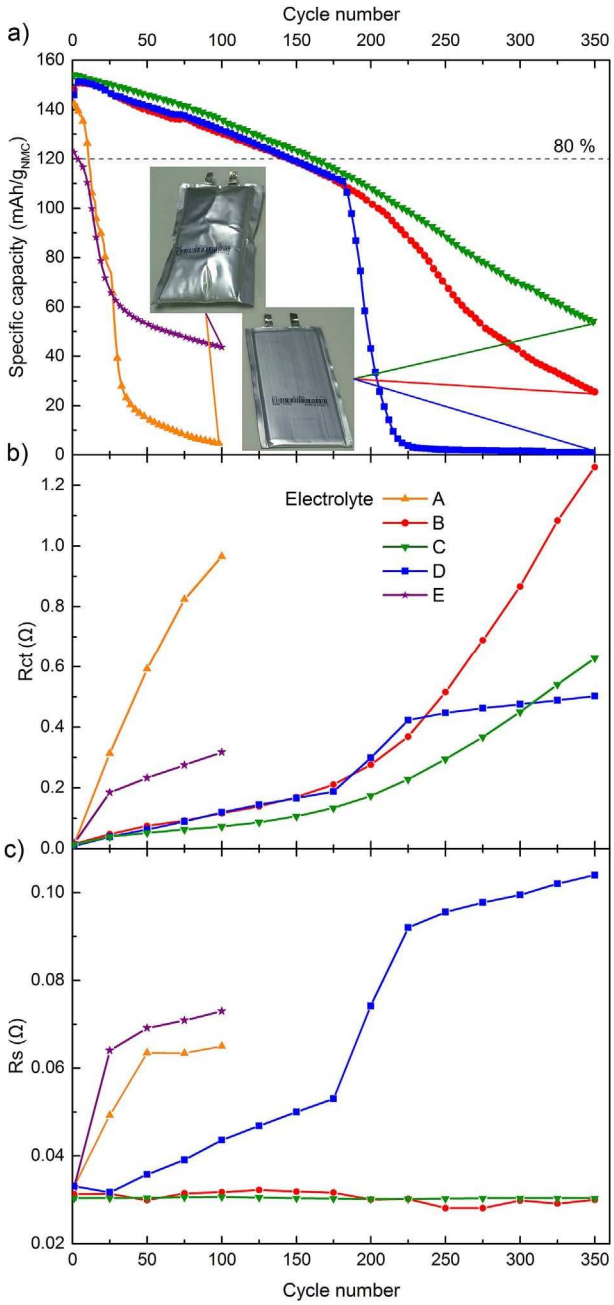

Fig. 1. a) Discharge capacity b) charge transfer resistance and c) series resistance over the cycle number of NMC/graphite pouch cells filled with different electrolyte compositions (see Table 1) and cycled at 80 °C – pouch cell images are representative for indicated electrolyte compositions.

3. Results and discussion

3.1. Cycle stability, resistance increase and volume expansion

Fig. 1a shows the cycling performance of pouch cells filled with different electrolytes and cycled at 80 °C. Batteries filled with the standard electrolyte A, with no additional additives lose up to 90% of their initial capacity within the first 25 cycles. They also show an excessive amount of cell swelling. It is believed that the conductive salt $LiPF_6$ decomposes at elevated temperatures to form LiF and PF_5 [42]. The latter product is a strong Lewis acid which can react with water to form HF and POF_3, but it was also reported to induce reactions with

organic solvents to form different types of polymers (e.g. polyethyleneoxide - PEO) and CO_2 [43,44].

$$LiPF_6 \xrightarrow{\Delta T} LiF + PF_5$$

$$PF_5 + H_2O \rightarrow 2HF + POF_3$$

$$C_3H_4O_3\ (EC) \xrightarrow{PF_5/POF_3} PEO + CO_2$$

Additionally a cathode-induced oxidation of the solvents will lead to gas generation, including CO, CO_2 and other products [45,46]. Detailed mechanism for the reaction of PF_5 with solvent molecules and oxidation induced reactions of carbonate esters are described by Xing et al. and Wilken et al. [45–47]. By adding 1% of VC to the standard electrolyte (Fig. 1a - Curve B) the cycle performance was greatly improved. Due to its double bound this additive is mainly known for its reductive behaviour to build a more stable, anodic SEI layer [48–50]. However it is also believed to form a thin, polymeric decomposition film at the cathode interface, thus increasing the oxidation stability for solvents [51]. Electrolyte composition C was identified to improve the cycling performances at 55 °C.

Xia et al. showed that NMC pouch cells can exhibit a capacity retention of around 88% after 1000 cycles at this temperature [39]. However, when cycling cells with this composition at 80 °C, only a slightly better performance was observed, compared with batteries using formulation B (1% of VC). Cells with electrolyte D displayed a similar capacity fade during the first 200 cycles, but showed a 'roll over' effect afterwards, where an abrupt capacity fade occurs within a few cycles (see Burns et al.) [23]. This observation was repeated at ≈ 250 ± 50 cycles. However, reproductions are deliberately not shown to display clearer relevant chart features. Electrolyte composition E contains 15% FEC which is a common portion for silicon containing batteries [52]. In these cells it is a necessary additives as it is able to increase the amount of LiF within the anode SEI which increases the mechanical stability of the decomposition film [53,54]. In low quantities FEC is known as an additive which can improve the cycle stability at elevated temperatures [55]. However, in this study NMC/graphite cells with electrolyte E also show a premature capacity fade and cell swelling within the first 25 cycles. This might be due to a thermal decomposition of FEC (e.g. de-hydro-fluorination) which also results in higher HF contents at elevated temperatures [54,56].

$$C_3H_3O_3F\ (FEC) \xrightarrow{\Delta T} HF + C_3H_2O_3\ (VC)$$

The fitting results of the charge transfer resistance (R_{ct}) over the cycle life at 80 °C are displayed in Fig. 1b. The increase is non-linear which might be explained by the CC-CV charge mode. At high cell voltages the resistance increase is believed to be accelerated. During the constant voltage phase the battery remains at these potentials for a longer time to reach the same cut-off current. It can be observed that the charge transfer resistance of cells with electrolyte C does not grow as fast as in the case for cells with composition B. This is possibly related to an increase in the oxidation stability of the solvents by the use of PES as an additive although, the trend of the increase is similar. When compared with a cycling study including the same electrode materials and electrolyte formulation (NMC-graphite, electrolyte C), the resistance increase was much lower at 55 °C [39]. The series resistance fits, which are displayed in Fig. 1c are almost constant for batteries with the electrolyte composition B and C. Cells with these electrolytes are the only ones that retained a liquid phase when opened under argon, following high temperature cycling. Therefore the increase in series resistance is indicative for the decomposition of the electrolyte. Cells with electrolyte D show a linear increase of Rs until the start of the capacity 'roll over'. At this point it seems likely that most of the electrolyte was consumed, resulting in a stepwise increase of the charge transfer and series resistance. This behaviour is likely related to the different solvents, owing to similar additives consistent with

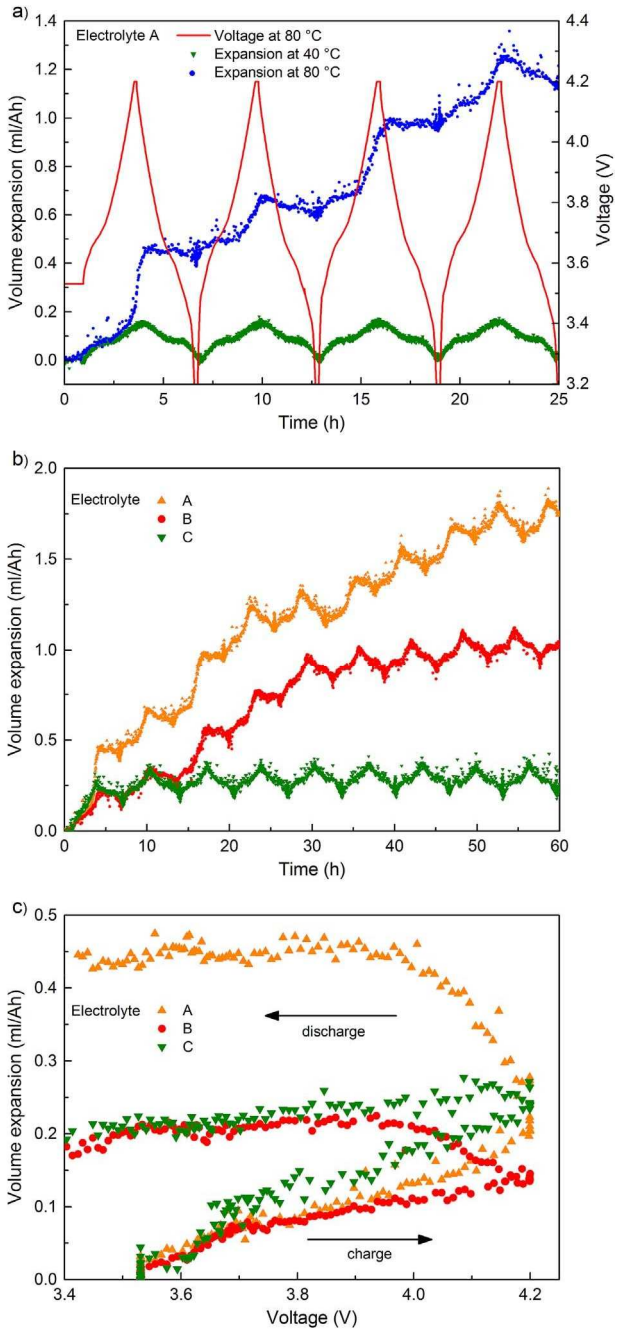

Fig. 2. a) Volume expansion and voltage over time for cells cycled with electrolyte A at 40 and 80 °C b) volume expansion for cells with different electrolytes (see Table 1) at 80 °C c) initial volume expansion during the first cycle with different electrolytes at 80 °C.

formulations B and C being used. Propylene carbonate (PC) is known for solvent co-intercalation into the graphite structure [57,58] and diethyl carbonate (DEC) showed lower oxidation stabilities in $LiPF_6$ based mixtures [59]. Both ageing effects might be accelerated at elevated temperatures.

The cell images in Fig. 1a show that the stepwise increase of the resistance is not connected with an excessive amount of gas generation as it is the case for cells with electrolyte A and E, suggesting a different degeneration process. Fig. 2a shows the initial voltage profile as well as the in-situ volume expansion of cells filled with the standard electrolyte A, cycled at 40 and 80 °C. The repeated expansion and contraction baseline at lower temperatures exists due to the volume change of both electrode active materials. It is connected to a change in the lattice parameters of the intercalation materials during lithium insertion and

extraction [40,60–63]. Typical expansion values of electrodes are ≈8% during the lithiation of graphite and ≈2% for the delithiation of transition metal oxides [64]. For cells incorporating the standard electrolyte there is an additional volume increase at elevated temperatures. The onset occurs at approximately 3.9 V during the charge with a decline at a similar potential during the discharge. It is well known that the anode potential in this area is almost constant. We can therefore conclude that an oxidation reaction with gaseous products on the cathode side must be responsible for the volume expansion of the pouch cells. This has been confirmed by Onuki using ^{13}C-labeled solvents [65]. Product gases mainly consist of CO and CO_2, generated by an oxidative decomposition of the solvents. EC is regarded to be the main source of these gases, as it has been reported that cyclic carbonates were more reactive then aliphatic ones [65]. The volume expansion profile between cells filled with electrolyte A, B and C (cycled at 80 °C) is displayed in Fig. 2b.

Batteries containing electrolyte B (standard + 1% VC) show a delayed expansion onset compared to the electrolyte without additives (composition A). This is likely to be due to the passivating effect of a stable decomposition layer by VC. The expansion onset for cells filled with electrolyte composition C occurs at around 3.7 V as shown in Fig. 2c. This occurrence is prior to the gas generation for cells filled with the standard electrolyte with no additives. However, following the expansion during the first two cycles no further gas generation was observed. This could be an indication that decomposition products from sulfur based additives (as PES or DTD) generate a more stable surface layer on the cathode interface and prevent a further oxidation of solvents. An indication for this behaviour could be the verification of R-SO_3Li species on both electrode interfaces, after storing NMC cells with 2% propane sultone (PS) at 75 °C [38]. The effect of TTSPi, which is a Lewis-base should also be considered. Other chemicals with an analogous structure are known as $LiPF_6$ salt stabilizers and act by reducing the reactivity and acidity of PF_5, therefore preventing additional HF and gas generation as described above [50]. It is further noted that more gas is generated during the discharge than during the charge but the potential range remains consistent.

3.2. SEM characterisation of electrodes

Fig. 3a shows SEM images of the cathode composites after cycling at 25 and 80 °C with electrolytes A and C. Micrographs of both pristine electrodes can be found in Fig. S2. It is apparent that a thick film of decomposition products is formed when NMC cells are aged at elevated temperatures and without additives. A possible component could be polyethylene carbonate, as it was also found on the surface of different cathode materials aged at 60 °C [66]. The image features for electrolyte C are representative for the rest of the electrolyte formulations (B to E). In contrast to cells with the standard electrolyte (A) no change in surface morphology was observed. However, it does not follow that electrolytes with these additives prevent solvent oxidation. As reported by Burns et al. and Xiong et al. soluble oxidation products can be formed at the cathode and migrate to the negative electrode [21,23]. Here they can be reduced to form a growing SEI layer or constitute additional gaseous products. SEM micrographs of the 25 and 80 °C aged anode composites with different electrolytes are shown in Fig. 3b.

It was observed that cycling at elevated temperatures changed the surface morphology of these electrodes similar to findings from Andersson and Edström [18]. When no additives were used, a thick crystalline like layer covered the particles. The majority of these crystals consist of LiF, as Bodenes et al. reported that compounds such as carbonates disappear from the anode surface when electrodes were cycled above 60 °C [36]. It has yet to be clarified whether these compounds become dissolved in the electrolyte or if a new decomposition layer grows on top. A smaller amount of particle coverage and crystallite size was observed for cells with electrolyte B and E. It can be concluded that by using these formulations either a more stable anodic SEI was formed or that less material was oxidized at the cathode interface and transported to the anode. A different kind of morphology was observed on anodes from cells with electrolyte D. Blossom shaped crystals covered the surface of the graphite particles, which did not dissolve upon washing with DMC. This eliminates the possibility of crystalized $LiPF_6$. An explanation for this phenomenon might be a gentle decomposition of the conductive salt whilst the solvents are slowly consumed. The increase of the series resistance (Fig. 1c) for cells with electrolyte D supports this theory. Cells with the electrolyte formulation C were the only ones to show a similar surface morphology when compared with cells cycled at 25 °C. Overall it could be assumed that the resistance increase, which was observed during the cycling at elevated temperatures, is connected to the change of the anode morphology as suggested by Bodenes et al. or Jalkanen et al. [36,67]. However, the following results will show that the cathode is more accountable.

3.3. Symmetrical EIS and half-cell results

Fig. 4a shows Nyquist plots of symmetrical cathode coin cells with electrolyte C, having undergone different ageing conditions. Electrodes from cells which were aged at 80 °C demonstrated a charge transfer resistance twenty five times larger than the ones following formation. By contrast, cathodes aged for the same number of cycles at room temperature showed a doubling of resistance. Yet in the case of the anode (Fig. 4b) the resistance grows only slightly during the 25 °C cycling and even decreases in pouch cells cycled at 80 °C. Especially the first semicircle at high frequencies seems to be smaller. This area is reported to be connected with the SEI resistance [68]. A reduction in this range could be related to the disappearance of carbonate species from the graphite surface, as mentioned in the previous section. In Fig. 4c it can be seen that different electrolyte formulations lead to varying degrees of resistance increase for the cathodes. For cells without additional additives (composition A) this could be explained by the visible decomposition layer on the positive electrode surface. However, the largest resistance increase was measured for cells with electrolyte B, containing 1% VC. The difference can be explained by the variation in the number of cycles undergone by these cells at 80 °C.

Whilst cells with electrolyte B were running for 350 cycles, those with composition A lost more than 90% of their initial capacity during the first 100 cycles (see Fig. 1a). Based on the diverse amount of gas generated, we assume that the resistance increase for these cells follows a different degradation mechanism. A small amount of VC can impede the initial solvent oxidation seen in cells with the standard electrolyte but it cannot fully mitigate the mechanism which increases the cathode resistance over the subsequent number of cycles. Cells filled with electrolyte C experience a slow-down of this second type of degradation but they ultimately follow the same trend. A lower resistance for symmetrical cells with electrolyte D (Fig. 4c) is therefore most likely connected to the abrupt capacity fade. Cathodes from cells with this electrolyte formulation might undergo an increase in resistance only during the first 175 cycles before the degradation of the electrolyte leads to an accelerated capacity loss. Similar rules apply for cathodes from cells incorporating electrolyte E, which show the lowest resistance increase of all cathodes aged at 80 °C. Due to the early capacity loss of these cells, almost no additional cathode resistance was developed. Compared with the significant alterations in the positive electrode resistance, the influence of the electrolyte is smaller for the negative electrode - as can be seen in Fig. 4d. Differences between electrolyte formulations could certainly be explained by the observed changes in surface morphology (Fig. 3b). Thick decomposition films formed on anodes from cells with compositions A and D result in larger charge transfer resistances than it is the case for other formulations. Fig. 4e and f shows half-cell voltage profiles of cathodes and anodes aged at 80 °C. A reduction of the specific capacity, which can be observed for positive electrodes, is also related to an increase in resistance and therefore the voltage hysteresis. Hence, batteries with a large cell resistance reach the

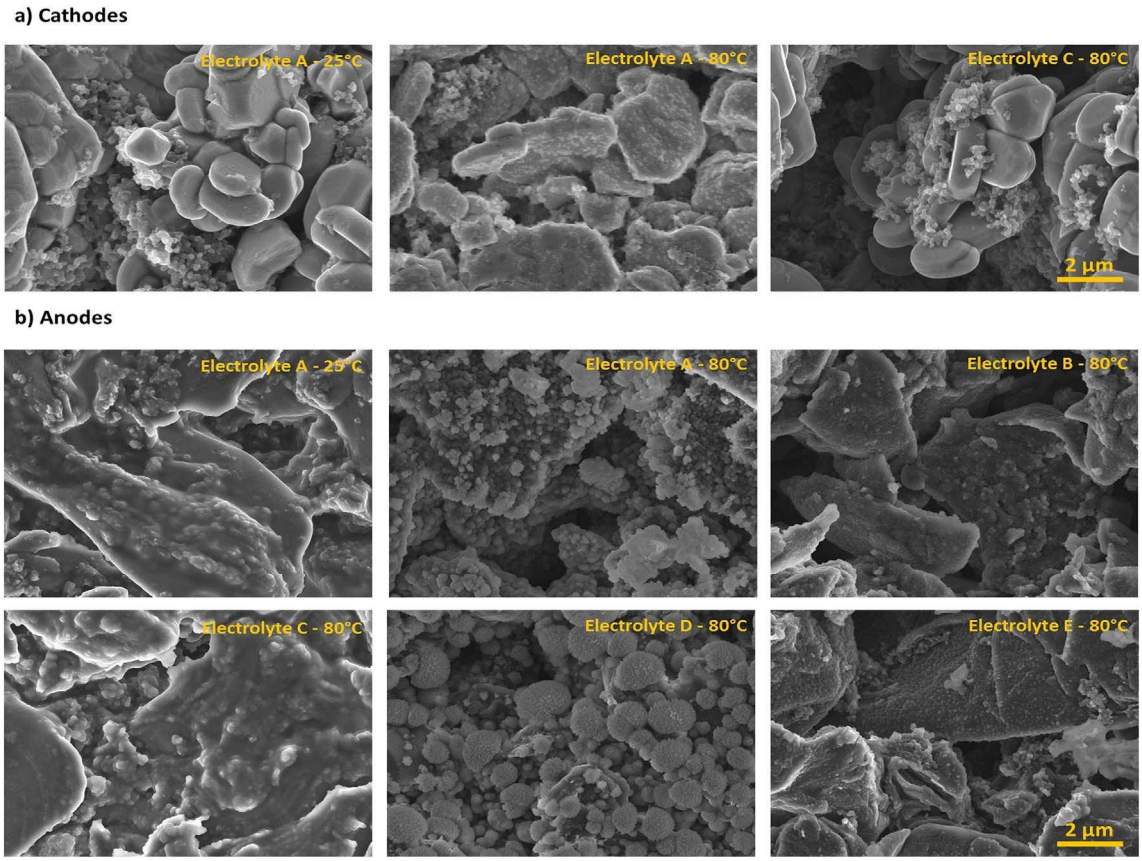

Fig. 3. SEM micrographs of NMC cathodes (a) and graphite anodes (b) cycled in pouch cells at 25 °C and 80 °C with different electrolyte compositions (A – E, see Table 1).

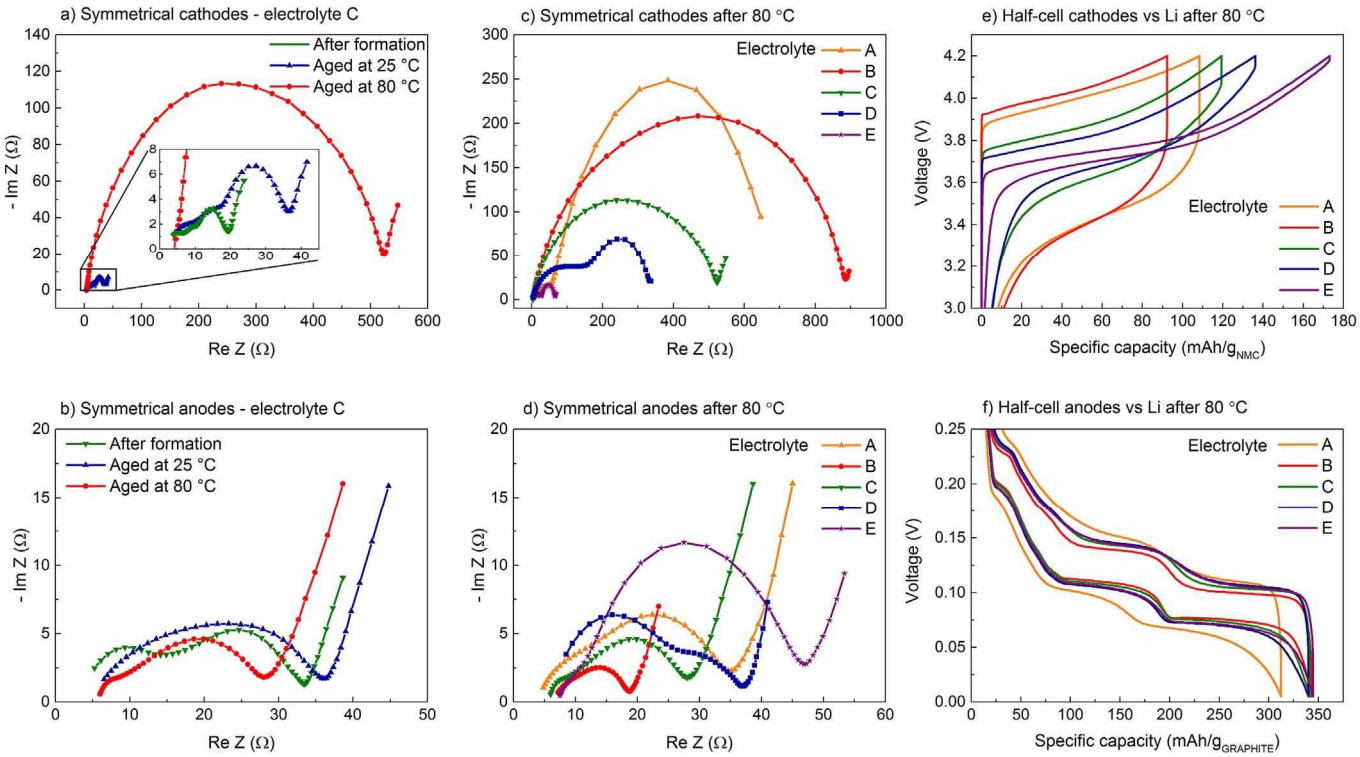

Fig. 4. a,b) Nyquist plots of symmetrical cathode and anode coin cells with electrolyte C, aged under different conditions c,d) Nyquist plots of symmetrical cathode and anode coin cells with different electrolytes formulations (see Table 1) aged at 80 °C e,f) half-cell voltage profiles vs. Li/Li$^+$ of cathodes and anodes aged with different electrolytes at C/20 – all measurements were done at 25 °C.

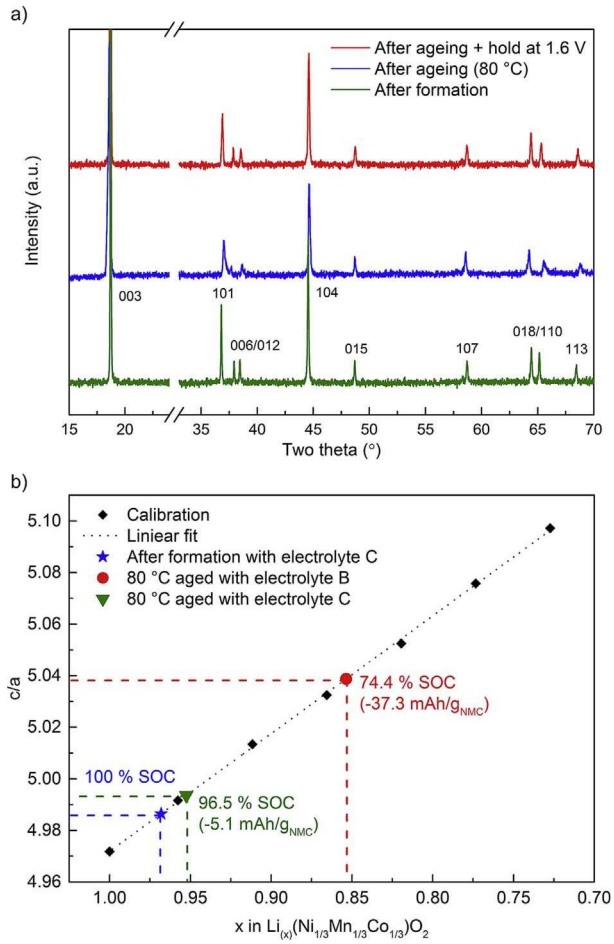

Fig. 5. a) XRD pattern of NMC cathodes with electrolyte C, after the formation and aged at 80 °C, discharged to 3.5 V and held at 1.6 V b) fitted a/c lattice ratio in hexagonal space group as a function of x in $Li_{(x)}(Ni_{1/3}Mn_{1/3}Co_{1/3})O_2$ for pristine and fresh cells charged to different SoC (lithium contents).

cut-off voltage sooner. The capacity sequence for cathodes aged with different electrolyte formulations agrees herein with the resistance observed from Nyquist plots. Different anode half-cells do not show large changes in the voltage hysteresis and specific capacity except for those aged with electrolyte A. Anodes from cells aged with this formulation also showed an excessive amount of electrode delamination from the copper current collector. All coin cells were cycled with the same current rather than being adjusted relative to the mass of active material. Therefore a lower amount of graphite would lead to a higher C-rate and a larger voltage hysteresis/less capacity.

3.4. Structural characterisation and lithium content by XRD

In order to find out more about the process of the cathode degradation, XRD was performed on fresh and aged electrodes. Fig. 5a shows the diffraction pattern of electrodes with electrolyte C before and after the ageing at 80 °C. The hkl values are related to the hexagonal $R\bar{3}m$ space group of the NMC lattice. Following high temperature degradation, no additional bulk phases were found and this was also the case for cathodes from cells with other electrolytes. This finding agrees with literature on similar ageing studies [67,69,70].

A minor amount of peak broadening can be explained by lattice distortions linked to the "platelet" and "strain" effect (see R. Hausbrand et al.) [63]. These distortions are considered highly reversible and are therefore not related to a large fatigue contribution of the active material. However, a clear change of diffraction positions was observed between fresh and aged electrodes discharged to 3.5 V. These shifts are well observed for hkl values of 006/012 and 018/110 and relate to a change of the lattice parameters a and c. It is known that the volume of the NMC unit cell changes during the intercalation and deintercalation of lithium ions [63,70]. When opening fresh and aged pouch cells they are likely to be at different lithiation levels, even when discharged to the same cut off potential. This is due to differences in cell resistance and voltage hysteresis as shown previously. Buchberger et al. showed that a change in the a/c ratio is linear over the lithium content of NMC and can be used to calculate the amount of active lithium within a cell [70]. Fig. 5b shows such a calibration of a/c values over the lithium content for the cathode material used in this study. They also revealed that NMC held at 1.6 V vs. Li is able to restore approximately all of its missing lithium without showing changes in the bulk phase. The diffractogram of an 80 °C aged cathode with electrolyte C and held for 12 h at 1.6 V is shown in Fig. 5a. No additional diffraction lines are observed here and the peak broadening seems to be decreased. By using Rietveld refinement the a/c ratio for the lattice parameters of these electrodes were calculated. As shown in Fig. 5b, the ratio of 4.994 equals to a lithium amount of $x \approx 0.952$, stating that most of the active lithium inside the aged cells (Electrolyte C) is still available. This would relate to a remaining SoC value of ≈96.4%. One could argue that additional Li ions from the electrolyte or other sources (decomposition of SEI) were used to take part in the reintercalation of Li into the cathode. However, when applying the same procedure on a cell after the formation, an a/c ratio of 4.986 was obtained. This relates to a Li value of $x \approx 0.968$. The difference to $x = 1$ agrees well with first cycle loss during the formation of the SEI. Therefore, we imply that it is unlikely that lithium from sources other than graphite was intercalated. When comparing the a/c ratio of cathodes with the electrolyte containing 1% VC (electrolyte B) and the electrolyte composition for high temperatures (electrolyte C) a larger number of 5.039 was obtained. This shows that a much greater fraction of Li is lost due to parasitic side reactions (≈74.4% SoC remaining). The a/c ratio of cathodes aged with the unaccounted electrolytes (composition A, D and E) was high enough to be out of the SoC calibration range (c/a > 5.10), indicating an even larger proportion of Li loss. Considering the XRD results from cells with electrolyte C, we learned that almost all of the active Li inside the cells is still available after 350 cycles at 80 °C (SoC value of ≈96.4%). However the measured discharge capacity at this point is ≈ 55 mAh g_{NMC}-1(SoC value of ≈35%). The difference can be explained by the resistance increase, which results in an enormous voltage hysteresis. The origin of this additional resistance was found to be primarily cathode related, yet XRD measurements confirmed that the bulk structure of the NMC cathode material does not change.

3.5. Cathode surface analyses by XPS

In order to investigate the reason behind the resistance increase for cathodes with electrolyte C, XPS was performed on electrodes aged at 25 and 80 °C. C 1s spectra of these samples can be seen in Fig. 6a and b and spectra related to the pristine cathode are shown in Fig. S3. The intense signal at 284.8 eV is assigned to the conductive additive (C-C) while two other peaks at 286.2 and 290.7 eV are related to $-CH_2-$ and $-CF_2-$ from the PVDF binder. Other carbon signals are connected to oxygenated environments like C-O, C=O and CO_3 [36,37]. As a results of the ageing at elevated temperatures a clear intensity increase for these substances can be observed.

Much reported research connects this change to a thickness increase of the decomposition layer on the cathode surface, but also the conductive carbon (which covers a large amount of the electrode interface) should be considered here, as it shows a similar surface chemistry [36,71,72]. Younesi et al. showed that electrodes which were based only on conductive carbon and binder generate an increase in oxidized species when cycled at high potentials [71]. Additionally, storage experiments at 40 °C in $LiPF_6$ based electrolytes lead to the formation of ether based species (C-O) [71]. Therefore, we believe that the cycling of

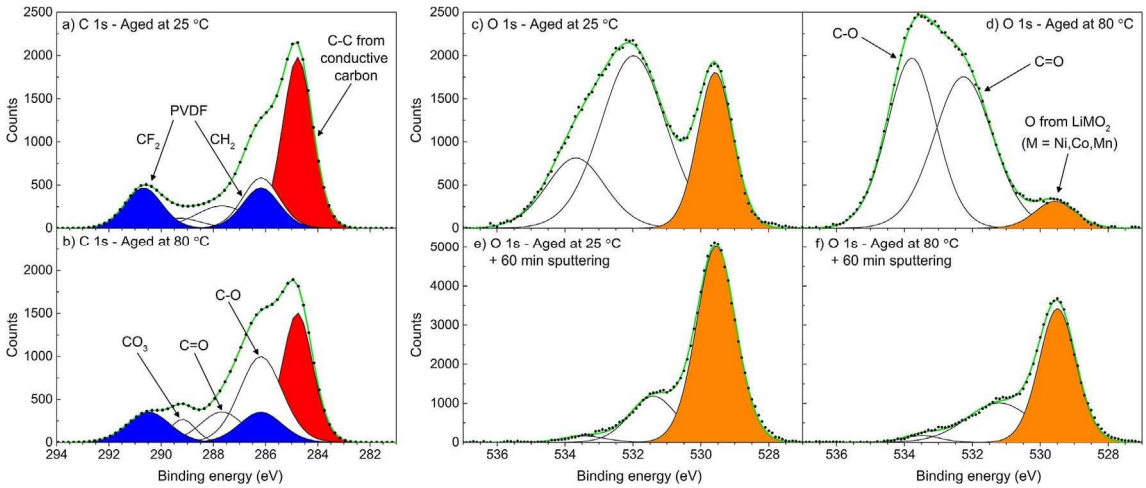

Fig. 6. C 1s (a,b) and O 1s (c-f) XPS spectra of NMC cathodes cycled at 25 °C and 80 °C with electrolyte C (see Table 1).

conductive additives at elevated temperatures will also result in an increase of carbon-oxygen compounds on its surface. Yet, to our knowledge, tests in this direction still have to be comprehensively performed and understood.

Fig. 6c–f shows O 1s core peaks of differently aged positive electrodes before (c, d) and after (e, f) 60 min of Ar-ion sputtering. Cells which were aged at 25 and 80 °C showed two major differences. Firstly, the reduction of the peak related to metal-oxygen bonds at 529.5 eV and secondly the increase of C-O related species at 533.8 eV [36,73]. The signal around 532 eV, which barely changes in intensity, is attributed to C=O species as reported from Li_2CO_3 and polycarbonates [73,74]. The metal-oxygen peak is related to the oxygen within the NMC structure and a decrease in its intensity is therefore attributed to the growth of the decomposition layer [36]. The increase upon ageing at elevated temperatures arises mainly from C-O species as found in PEO and further polyether. Other oxygen containing compounds like $Li_xPO_yF_z$ have not been included, as only small amounts of phosphorus bounds were detected. It was reported that the decomposition film on the cathode interface is likely to be smaller than 5–10 nm when metal-oxygen bonds are still detected [36]. This is based on the XPS depth of analysis which changes for different surface chemistries. However, a second interpretation could also be an inhomogeneous film covering of the particle surface. After 60 min of Ar^+ sputtering most of the surface species have disappeared from both samples with the oxygen-metal peak gaining in intensity. Yet, compared with the electrodes that were aged at 25 °C, those cycled at elevated temperatures still show a lower signal at 529.6 eV. It would be misleading to conclude that a major loss of oxygen from the bulk structure is the reason for this finding, as the XRD pattern did not show any additional diffraction lines for these samples. We therefore conclude that the oxygen reduction could be related to a growing reconstruction layer on the NMC particle surface.

3.6. Cathode reconstruction layer analyses using STEM and EELS

Fig. 7a displays a high resolution annular dark field (HR-ADF) STEM image over the cathode surface of an electrode aged at 80 °C with electrolyte C. The upper left corner of this image shows electron deposited platinum particles that have been applied to protect the NMC particle surface from the Ga^+ ions during FIB sample thinning. The contrast increase close to the NMC particle edge is caused by a larger amount of transition metals within a reconstruction layer. However, this change in contrast could also occur due to a variable sample thickness over the acquired imaging area. Other research groups presented Z-contrast HR-STEM images of NMC particles along the $R\bar{3}m$ [100] zone axis in combination with nano-beam diffraction, indicating a $Fm\bar{3}m$ rock-salt-type reconstruction layer [34,75,76]. The intercalation axis was not visually obtained in this study as samples were ≈150 nm in thickness, too high for good atomic resolution imaging. A major disintegration of secondary particles occurred when thinned further. However, EELS line scans were performed over the particle edge of the samples for further analyses of the reconstruction layer. Fig. 7b shows an EELS spectra from the bulk of the 80 °C aged NMC sample. The magnified Mn, Co and Ni L-edge EELS spectra for position A and B of the line scan are displayed in Fig. 7c. A clear shift to lower energy losses of the Mn and Co L_3 and L_2-edges was observed for spectra within the high contrast line. The position of L-edges for transition metals is associated to the change of electrons from 2p core states to 3d states [75].

The shift to lower energies correlates with a minor oxidation state of Mn and Co atoms but is absent for the Ni L-edge. This is due to the fact that the oxidation state of Ni is already +2 within the bulk structure of pristine NMC [75]. Fig. 7d shows the fitted peak positions of Mn, Co, and Ni L_3-edges over the grain boundary for differently aged NMC particles. The position of all line scans was determined by the ADF signal intensity. For both, Mn and Co L_3-edges a shift to lower energies was observed within the first 5 nm of the grain boundary, when cells where cycled at 25 or 80 °C. This agrees well with the estimated thickness of the altered layer from the ADF image. EELS line scans from pristine electrodes did not show a change of L_3-edge peak positions for these transition metals. Interestingly the thickness of the reconstruction layer did not increase when cells were aged at elevated temperatures. This could be due to an inhibiting effect of the PES additive as reported by Li et al. [76]. Therefore the oxygen loss observed for XPS spectra in Fig. 6f may not be directly related to the thickness of the reconstruction layer. However, Lin et al. found that the structural reconstruction at the particle surface is highly anisotropic and more pronounced along the Li-ion intercalation pathways [75]. Whereas Liu et al. stated that different levels of electrolyte exposure might play a more dominant role [34]. Due to the time-consuming specimen preparation only three areas within two different electrode regions have been analysed per cell. Within these samples our findings were reproducible.

3.7. Cathode SEM cross-sectional characterisation

Since no thickness increase of the reconstruction layer could be observed, another degradation mechanisms must be the driving force behind the growing resistance of cathodes aged with electrolyte C. Fig. 8a and b shows cathode cross-sections of samples, aged at 25 and 80 °C.

It is clearly visible that NMC secondary particles consists of many sintered single grains. Electrodes that were cycled at elevated temperatures show a clear disintegration of these. Both electrodes were

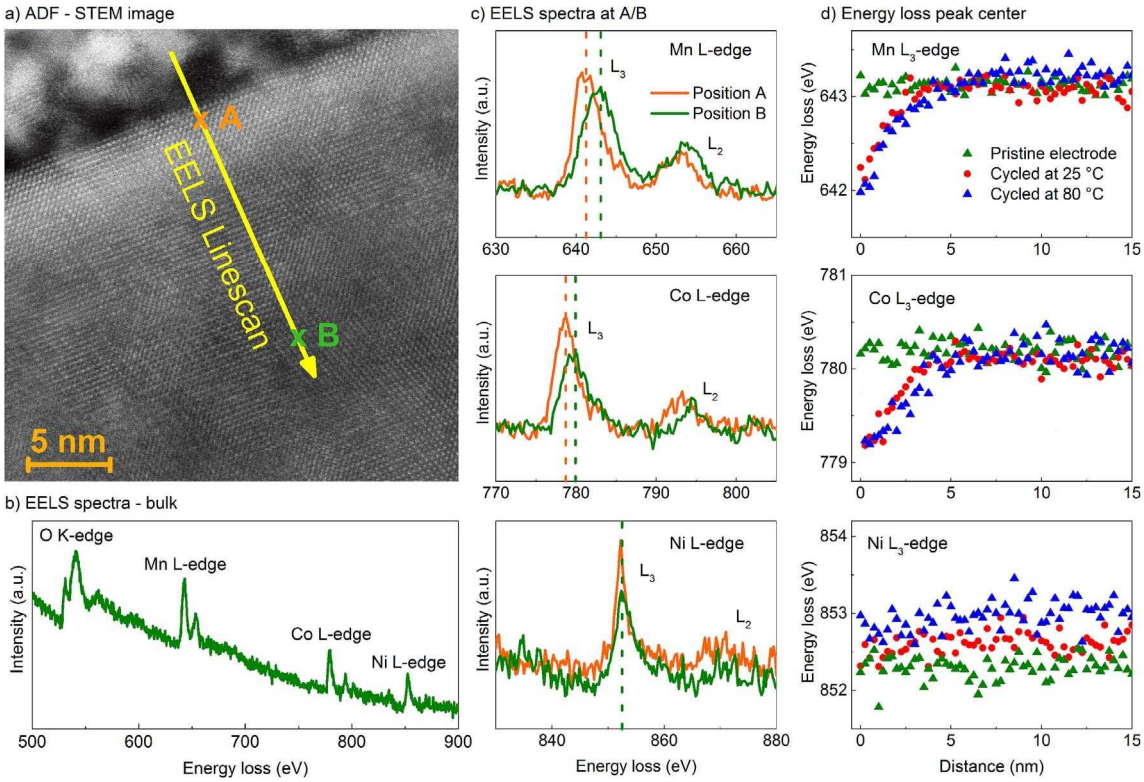

Fig. 7. a) High resolution annular dark field (HR-ADF) STEM image from the edge of a NMC particle aged at 80 °C with electrolyte C b) EELS spectra from indicated position B in the ADF image c) EELS spectra from positions A and B in the ADF image – zoomed into metal L-edge regions d) fitted peak positions of Mn, Co, and Ni L_3-edges of EELS line scans over the particle edge of different aged NMC electrodes with electrolyte C.

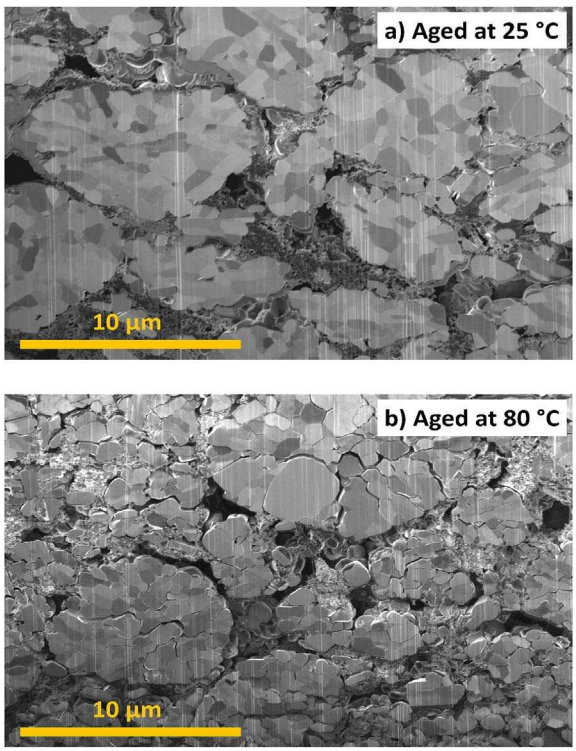

Fig. 8. FIB/SEM cross-sections of NMC electrodes from cells aged for 350 cycles with electrolyte C at 25 °C (a) and 80 °C (b).

cycled using the same C-rate. We can therefore discard the notion that this behaviour is connected to the volume expansion and contraction of the grains during normal insertion and extraction of lithium ions. To our knowledge, the following two effects might lead to the separation of primary particles. Firstly, there is a dissolution of transition metal ions at different cell voltages [70]. It is believed that these reactions are accelerated for both, high and low voltages, in the presence of HF and elevated temperatures [70]. Secondly, properties such as a lower viscosity and increased vapour pressure could enable the electrolyte to move into new nano pores and ingress between primary grains during their volume change. The later theory is supported by the fact that more capacity loss and particle cracking was observed when cycling cells over the full range of SOC (0–100%) and less when cycling just at high voltages (SoC 40–100%) or low voltages (SoC 0–60%) at 60 °C [77]. However, both paths would lead to the point where the electrolyte gets in contact with fresh active material. This would result in the formation of a new decomposition and reconstruction layer between primary particle grains. Such phenomena can lead to an increase in contact resistance and surface polarisation within the electrode [31]. EELS line scans over grain boundaries between separated primary particles confirmed the existence of reconstruction layers, albeit absent in regions where single grains were still in contact with each other.

Referring to the secondary NMC particles in Fig. 8, areas with conductive additive can be found. Interestingly the contrast of this component changed after the ageing at elevated temperatures (under similar acquisition settings). Due to charging effects, brighter areas may be indicative of a lowered electronic conductivity. It is reported that intercalation of PF_6^- into conductive carbon structures is possible at high voltages and elevated temperatures, leading to an increased number of structural defects [78]. Ruther et al. stated that this behaviour is also accompanied by a decrease of the Raman D/G band intensity ratio of carbon species [79]. They further claimed that an increase in structural defects might have a negative impact on the electronic conductivity of the cathode. Fig. S4 shows Raman spectra for the carbon D and G band area of different aged, positive electrodes. No major changes in cells aged at 25 and 80 °C or cells with different

electrolytes were found. These results do not agree with findings of Ruther et al. who showed a clear D/G ratio change after 50 cycles at 60 °C [79]. One of the main difference between both studies is a higher cut-off potential of 4.5 V for their cells. Syzdek et al. showed that pure conductive carbon electrodes can also exhibit a D/G ratio change when cycled at 45 °C up to 4.9 V [78]. It is therefore likely that the upper cut-off voltage has a larger impact than the temperature on the structural disorder of conductive carbons and a possible resistance increase of the cathode.

4. Conclusions

Industrially manufactured NMC/graphite cells with different electrolytes have been cycled at 80 °C. Using additive-free electrolytes or inappropriate additives, resulted in serious capacity fade and gas generation within the first 25 cycles. When more suitable electrolyte compositions were incorporated, the cycling performance was improved and the volume expansion was reduced. Formulations based on PES containing electrolytes (composition C – Table 1) showed an excellent cycling stability at 55 °C [39]. However, here we showed for the first time that at 80 °C these cells performed similarly to batteries with the standard electrolyte with only 1% VC (composition B). Around 80% capacity retention was observed within 200 cycles when using these compositions. The capacity fade was accompanied by a large resistance increase with the growth found to be predominantly cathode related. This dramatic resistance increase was not observed in similar ageing test at 55 °C [39]. XRD has been used to show that the bulk structure of the positive active material remained unchanged. Batteries aged with electrolyte C lost insignificant amounts of active lithium, equal to a capacity loss of ≈3.6%. The capacity loss during the cycling of cells with this electrolyte is therefore primarily based on the increase of the voltage hysteresis/loss of power. It was found that the thickness of a reconstruction layer at the cathode interface was subtly changing for electrodes cycled at 80 °C. However, a disintegration of secondary NMC particles led to additional decomposition and reconstruction layers between primary grain boundaries. This could essentially lead to the resistance increase observed during cycling. A connection between a possible conductivity loss of the cathodic carbon additive and the Raman D/G band ratio was not found. We suggest that an investigation on single grain cathode particles in combination with suitable electrolytes is a strategy to further improve the cycling performance of NMC/graphite based cells at elevated temperatures.

Acknowledgements

This work was supported by the High Value Manufacturing Catapult Centre and the Energy Innovation Centre, WMG at the University of Warwick.

Appendix A. Supplementary data

Supplementary data related to this article can be found at http://dx.doi.org/10.1016/j.jpowsour.2017.11.014.

References

[1] X. Lin, M. Salari, L. Mohana, R. Arava, P.M. Ajayan, M.W. Grinstaff, High temperature electrical energy storage: advances, challenges, and frontiers, Chem. Soc. Rev. 45 (2016) 5848–5887, http://dx.doi.org/10.1039/C6CS00012F.

[2] K.H. Lee, E.H. Song, J.Y. Lee, B.H. Jung, H.S. Lim, Mechanism of gas build-up in a Li-ion cell at elevated temperature, J. Power Sources 132 (2004) 201–205, http://dx.doi.org/10.1016/j.jpowsour.2004.01.042.

[3] N. Yabuuchi, T. Ohzuku, Electrochemical behaviors of LiCo1/3Ni1/3Mn1/3O2 in lithium batteries at elevated temperatures, J. Power Sources 146 (2005) 636–639, http://dx.doi.org/10.1016/j.jpowsour.2005.03.080.

[4] h. Hussain, M. Al-Kayiem, Firdaus Bin M. Sidik, Yuganthira R.A.L. Munusammy, Study on the thermal accumulation and distribution inside a parked car cabin, Am. J. Appl. Sci. 6 (2015) 784–789.

[5] X. Feng, M. Fang, X. He, M. Ouyang, L. Lu, H. Wang, M. Zhang, Thermal runaway features of large format prismatic lithium ion battery using extended volume accelerating rate calorimetry, J. Power Sources 255 (2014) 294–301, http://dx.doi.org/10.1016/j.jpowsour.2014.01.005.

[6] C.Y. Jhu, Y.W. Wang, C.Y. Wen, C.M. Shu, Thermal runaway potential of LiCoO2 and Li(Ni1/3Co1/3Mn1/3)O2 batteries determined with adiabatic calorimetry methodology, Appl. Energy 100 (2012) 127–131, http://dx.doi.org/10.1016/j.apenergy.2012.05.064.

[7] A.W. Golubkov, D. Fuchs, J. Wagner, H. Wiltsche, C. Stangl, G. Fauler, G. Voitic, A. Thaler, V. Hacker, Thermal-runaway experiments on consumer Li-ion batteries with metal-oxide and olivin-type cathodes, RSC Adv. 4 (2014) 3633–3642, http://dx.doi.org/10.1039/C3RA45748F.

[8] Y. Wang, J. Jiang, J.R. Dahn, The reactivity of delithiated Li(Ni1/3Co1/3Mn1/3)O2, Li(Ni0.8Co0.15Al0.05)O2 or LiCoO2 with non-aqueous electrolyte, Electrochem. Commun 9 (2007) 2534–2540, http://dx.doi.org/10.1016/j.elecom.2007.07.033.

[9] H.F. Xiang, H. Wang, C.H. Chen, X.W. Ge, S. Guo, J.H. Sun, W.Q. Hu, Thermal stability of LiPF6-based electrolyte and effect of contact with various delithiated cathodes of Li-ion batteries, J. Power Sources 191 (2009) 575–581, http://dx.doi.org/10.1016/j.jpowsour.2009.02.045.

[10] K. Zaghib, M. Dontigny, P. Perret, A. Guerfi, M. Ramanathan, J. Prakash, A. Mauger, C.M. Julien, Electrochemical and thermal characterization of lithium titanate spinel anode in C-LiFePO4//C-Li4Ti5O12 cells at sub-zero temperatures, J. Power Sources 248 (2014) 1050–1057, http://dx.doi.org/10.1016/j.jpowsour.2013.09.083.

[11] S. Ma, H. Noguchi, High temperature electrochemical behaviors of ramsdellite Li2Ti3O7 and its Fe-doped derivatives for lithium ion batteries, J. Power Sources 161 (2006) 1297–1301, http://dx.doi.org/10.1016/j.jpowsour.2006.06.017.

[12] M. Dubarry, B.Y. Liaw, M.S. Chen, S.S. Chyan, K.C. Han, W.T. Sie, S.H. Wu, Identifying battery aging mechanisms in large format Li ion cells, J. Power Sources 196 (2011) 3420–3425, http://dx.doi.org/10.1016/j.jpowsour.2010.07.029.

[13] K. Amine, J. Liu, I. Belharouak, High-temperature storage and cycling of C-LiFePO4/graphite Li-ion cells, Electrochem. Commun. 7 (2005) 669–673, http://dx.doi.org/10.1016/j.elecom.2005.04.018.

[14] S. ichi Tobishima, K. Takei, Y. Sakurai, J. ichi Yamaki, Lithium ion cell safety, J. Power Sources 90 (2000) 188–195, http://dx.doi.org/10.1016/S0378-7753(00)00409-2.

[15] R. a. Leising, M.J. Palazzo, E.S. Takeuchi, K.J. Takeuchi, Abuse testing of lithium-ion batteries: characterization of the overcharge reaction of LiCoO[sub 2]/graphite cells, J. Electrochem. Soc. 148 (2001) A838, http://dx.doi.org/10.1149/1.1379740.

[16] C.Y. Jhu, Y.W. Wang, C.M. Shu, J.C. Chang, H.C. Wu, Thermal explosion hazards on 18650 lithium ion batteries with a VSP2 adiabatic calorimeter, J. Hazard. Mater 192 (2011) 99–107, http://dx.doi.org/10.1016/j.jhazmat.2011.04.097.

[17] C.Y. Wen, C.Y. Jhu, Y.W. Wang, C.C. Chiang, C.M. Shu, Thermal runaway features of 18650 lithium-ion batteries for LiFePO 4 cathode material by DSC and VSP2, J. Therm. Anal. Calorim. 109 (2012) 1297–1302, http://dx.doi.org/10.1007/s10973-012-2573-2.

[18] A.M. Andersson, K. Edström, chemical composition and morphology of the elevated temperature SEI on graphite, J. Electrochem. Soc. 148 (2001) A1100, http://dx.doi.org/10.1149/1.1397771.

[19] J. Shim, R. Kostecki, T. Richardson, X. Song, K.A. Striebel, Electrochemical analysis for cycle performance and capacity fading of a lithium-ion battery cycled at elevated temperature, J. Power Sources 112 (2002) 222–230, http://dx.doi.org/10.1016/S0378-7753(02)00363-4.

[20] J. Li, J. Zhang, X. Zhang, C. Yang, N. Xu, B. Xia, Study of the storage performance of a Li-ion cell at elevated temperature, Electrochim. Acta 55 (2010) 927–934, http://dx.doi.org/10.1016/j.electacta.2009.09.077.

[21] D.J. Xiong, R. Petibon, M. Nie, L. Ma, J. Xia, J.R. Dahn, Interactions between positive and negative electrodes in Li-Ion cells operated at high temperature and high voltage, J. Electrochem. Soc. 163 (2016) A546–A551, http://dx.doi.org/10.1149/2.0951603jes.

[22] N.N. Sinha, A.J. Smith, J.C. Burns, G. Jain, K.W. Eberman, E. Scott, J.P. Gardner, J.R. Dahn, The use of elevated temperature storage experiments to learn about parasitic reactions in wound LiCoO2/Graphite cells, J. Electrochem. Soc. 158 (2011) A1194, http://dx.doi.org/10.1149/2.007111jes.

[23] J.C. Burns, a. Kassam, N.N. Sinha, L.E. Downie, L. Solnickova, B.M. Way, J.R. Dahn, Predicting and extending the lifetime of Li-Ion batteries, J. Electrochem. Soc. 160 (2013) A1451–A1456, http://dx.doi.org/10.1149/2.060309jes.

[24] D.J. Xiong, L.D. Ellis, R. Petibon, T. Hynes, Q.Q. Liu, J.R. Dahn, Studies of gas generation, gas consumption and impedance growth in Li-Ion cells with carbonate or fluorinated electrolytes using the pouch bag method, J. Electrochem. Soc. 164 (2017) 1–9, http://dx.doi.org/10.1149/2.1091702jes.

[25] H.H. Chang, C.C. Chang, C.Y. Su, H.C. Wu, M.H. Yang, N.L. Wu, Effects of TiO2 coating on high-temperature cycle performance of LiFePO4-based lithium-ion batteries, J. Power Sources 185 (2008) 466–472, http://dx.doi.org/10.1016/j.jpowsour.2008.07.021.

[26] D.J. Lee, B. Scrosati, Y.K. Sun, Ni3(PO4)2-coated Li[Ni 0.8Co0.15Al0.05]O2 lithium battery electrode with improved cycling performance at 55??C, J. Power Sources 196 (2011) 7742–7746, http://dx.doi.org/10.1016/j.jpowsour.2011.04.007.

[27] Y.S. Jung, A.S. Cavanagh, L.A. Riley, S.H. Kang, A.C. Dillon, M.D. Groner, S.M. George, S.H. Lee, Ultrathin direct atomic layer deposition on composite electrodes for highly durable and safe Li-Ion batteries, Adv. Mater 22 (2010) 2172–2176, http://dx.doi.org/10.1002/adma.200903951.

[28] H. Lee, M.G. Kim, J. Cho, Olivine LiCoPO4 phase grown LiCoO2 cathode material for high density Li batteries, Electrochem. Commun. 9 (2007) 149–154, http://dx.doi.org/10.1016/j.elecom.2006.08.058.

[29] S.B. Jang, S.H. Kang, K. Amine, Y.C. Bae, Y.K. Sun, Synthesis and improved electrochemical performance of Al (OH)(3)-coated Li Ni1/3Mn1/3Co1/3 O-2 cathode materials at elevated temperature, Electrochim. Acta 50 (2005) 4168–4173, http://dx.doi.org/10.1016/j.electacta.2005.01.037.

[30] T. Sasaki, S. Muto, Y. Sasano, K. Tatsumi, K. Horibuchi, Y. Takeuchi, Y. Ukyo, Capacity-Fading mechanisms of LiNiO[sub 2]-based lithium-ion batteries, J. Electrochem. Soc. 156 (2009) A289, http://dx.doi.org/10.1149/1.3076137.

[31] S. Muto, Y. Sasano, K. Tatsumi, T. Sasaki, K. Horibuchi, Y. Takeuchi, Y. Ukyo, Capacity-Fading mechanisms of LiNiO[sub 2]-based lithium-ion batteries, J. Electrochem. Soc. 156 (2009) A371, http://dx.doi.org/10.1149/1.3076137.

[32] Y. Kojima, S. Muto, K. Tatsumi, H. Kondo, H. Oka, K. Horibuchi, Y. Ukyo, Degradation analysis of a Ni-based layered positive-electrode active material cycled at elevated temperatures studied by scanning transmission electron microscopy and electron energy-loss spectroscopy, J. Power Sources 196 (2011) 7721–7727, http://dx.doi.org/10.1016/j.jpowsour.2011.05.017.

[33] G. Cherkashinin, M. Motzko, N. Schulz, T. Spath, W. Jaegermann, Electron spectroscopy study of Li[Ni,Co,Mn]O_2/electrolyte interface: electronic structure, interface composition, and device implications, Chem. Mater 27 (2015) 2875–2887, http://dx.doi.org/10.1021/cm5047534.

[34] H. Liu, M. Bugnet, M.Z. Tessaro, K.J. Harris, M.J.R. Dunham, M. Jiang, G.R. Goward, G.A. Botton, Spatially resolved surface valence gradient and structural transformation of lithium transition metal oxides in lithium-ion batteries, Phys. Chem. Chem. Phys. 18 (2016) 29064–29075, http://dx.doi.org/10.1039/C6CP05262B.

[35] H. Bang, D.-H. Kim, Y.C. Bae, J. Prakash, Y.-K. Sun, Effects of Metal Ions on the Structural and Thermal Stabilities of Li[Ni[sub 1−x−y]Co[sub x]Mn[sub y]]O[sub 2] (x+y≤0.5) Studied by in Situ High Temperature XRD, J. Electrochem. Soc. 155 (2008) A952, http://dx.doi.org/10.1149/1.2988729.

[36] L. Bodenes, R. Dedryvere, H. Martinez, F. Fischer, C. Tessier, J.-P. Peres, Lithium-ion batteries working at 85 C: aging phenomena and electrode/electrolyte interfaces studied by XPS, J. Electrochem. Soc. 159 (2012) A1739–A1746, http://dx.doi.org/10.1149/2.061210jes.

[37] L. Bodenes, R. Naturel, H. Martinez, R. Dedryvère, M. Menetrier, L. Croguennec, J.P. Pérès, C. Tessier, F. Fischer, Lithium secondary batteries working at very high temperature: capacity fade and understanding of aging mechanisms, J. Power Sources 236 (2013) 265–275, http://dx.doi.org/10.1016/j.jpowsour.2013.02.067.

[38] M. Xu, W. Li, B.L. Lucht, Effect of propane sultone on elevated temperature performance of anode and cathode materials in lithium-ion batteries, J. Power Sources 193 (2009) 804–809, http://dx.doi.org/10.1016/j.jpowsour.2009.03.067.

[39] J. Xia, L. Ma, J.R. Dahn, Improving the long-term cycling performance of lithium-ion batteries at elevated temperature with electrolyte additives, J. Power Sources 287 (2015) 377–385, http://dx.doi.org/10.1016/j.jpowsour.2015.04.070.

[40] C.P. Aiken, J. Xia, D.Y. Wang, D.A. Stevens, S. Trussler, J.R. Dahn, An apparatus for the study of in situ gas evolution in Li-Ion pouch cells, J. Electrochem. Soc. 161 (2014) A1548–A1554, http://dx.doi.org/10.1149/2.0151410jes.

[41] R. Petibon, C.P. Aiken, N.N. Sinha, J.C. Burns, H. Ye, C.M. VanElzen, G. Jain, S. Trussler, J.R. Dahn, Study of electrolyte additives using electrochemical impedance spectroscopy on symmetric cells, J. Electrochem. Soc. 160 (2013) A117–A124, http://dx.doi.org/10.1149/2.005302jes.

[42] H. Yang, G.V. Zhuang, P.N. Ross, Thermal stability of LiPF6 salt and Li-ion battery electrolytes containing LiPF6, J. Power Sources 161 (2006) 573–579, http://dx.doi.org/10.1016/j.jpowsour.2006.03.058.

[43] S.E. Sloop, J.B. Kerr, K. Kinoshita, The role of Li-ion battery electrolyte reactivity in performance decline and self-discharge, J. Power Sources 119–121 (2003) 330–337, http://dx.doi.org/10.1016/S0378-7753(03)00149-6.

[44] B. Ravdel, K.M. Abraham, R. Gitzendanner, J. DiCarlo, B. Lucht, C. Campion, Thermal stability of lithium-ion battery electrolytes, J. Power Sources 119–121 (2003) 805–810, http://dx.doi.org/10.1016/S0378-7753(03)00257-X.

[45] L. Xing, W. Li, C. Wang, F. Gu, M. Xu, C. Tan, J. Yi, Theoretical investigations on oxidative stability of solvents and oxidative decomposition mechanism of ethylene carbonate for lithium ion battery use, J. Phys. Chem. B 113 (2009) 16596–16602, http://dx.doi.org/10.1021/jp9074064.

[46] L. Xing, O. Borodin, Oxidation induced decomposition of ethylene carbonate from DFT calculations – importance of explicitly treating surrounding solvent, Phys. Chem. Chem. Phys. 14 (2012) 12838, http://dx.doi.org/10.1039/c2cp41103b.

[47] S. Wilken, M. Treskow, J. Scheers, P. Johansson, P. Jacobsson, Initial stages of thermal decomposition of LiPF6-based lithium ion battery electrolytes by detailed Raman and NMR spectroscopy, RSC Adv. 3 (2013) 16359–16364, http://dx.doi.org/10.1039/c3ra42611d.

[48] H. Haruna, S. Takahashi, Y. Tanaka, Accurate consumption analysis of vinylene carbonate as an electrolyte additive in an 18650 lithium-ion battery at the first charge-discharge cycle, J. Electrochem. Soc. 164 (2017) A6278–A6280, http://dx.doi.org/10.1149/2.0441701jes.

[49] R.D. Deshpande, P. Ridgway, Y. Fu, W. Zhang, J. Cai, V. Battaglia, The limited effect of VC in graphite/NMC cells, J. Electrochem. Soc. 162 (2014) A330–A338, http://dx.doi.org/10.1149/2.0221503jes.

[50] S.S. Zhang, A review on electrolyte additives for lithium-ion batteries, J. Power Sources 162 (2006) 1379–1394, http://dx.doi.org/10.1016/j.jpowsour.2006.07.074.

[51] R. Wang, X. Li, Z. Wang, H. Guo, J. Wang, T. Hou, Impacts of vinyl ethylene carbonate and vinylene carbonate on lithium manganese oxide spinel cathode at elevated temperature, J. Alloys Compd. 632 (2015) 435–444, http://dx.doi.org/10.1016/j.jallcom.2015.01.220.

[52] M.J. Loveridge, M.J. Lain, Q. Huang, C. Wan, A.J. Roberts, G.S. Pappas, R. Bhagat, Enhancing cycling durability of Li-ion batteries with hierarchical structured silicon–graphene hybrid anodes, Phys. Chem. Chem. Phys. 18 (2016) 30677–30685, http://dx.doi.org/10.1039/c6cp06788c.

[53] M. Klett, J.A. Gilbert, K.Z. Pupek, S.E. Trask, D.P. Abraham, Layered oxide, graphite and silicon-graphite electrodes for lithium-ion cells: effect of electrolyte composition and cycling windows, J. Electrochem. Soc. 164 (2017) A6095–A6102, http://dx.doi.org/10.1149/2.0131701jes.

[54] Y. Okuno, K. Ushirogata, K. Sodeyama, Y. Tateyama, Decomposition of the fluoroethylene carbonate additive and the glue effect of lithium fluoride products for the solid electrolyte interphase: an ab initio study, Phys. Chem. Chem. Phys. 18 (2016) 8643–8653, http://dx.doi.org/10.1039/C5CP07583A.

[55] M.H. Ryou, G.B. Han, Y.M. Lee, J.N. Lee, D.J. Lee, Y.O. Yoon, J.K. Park, Effect of fluoroethylene carbonate on high temperature capacity retention of LiMn2O4/graphite Li-ion cells, Electrochim. Acta 55 (2010) 2073–2077, http://dx.doi.org/10.1016/j.electacta.2009.11.036.

[56] H. Shin, J. Park, A.M. Sastry, W. Lu, Effects of fluoroethylene carbonate (FEC) on anode and cathode interfaces at elevated temperatures, J. Electrochem. Soc. 162 (2015) A1683–A1692, http://dx.doi.org/10.1149/2.0071509jes.

[57] J.O. Besenhard, M. Winter, J. Yang, W. Biberacher, Filming mechanism of lithium-carbon anodes in organic and inorganic electrolytes, J. Power Sources 54 (1995) 228–231, http://dx.doi.org/10.1016/0378-7753(94)02073-C.

[58] G.-C. Chung, H.-J. Kim, S.-I. Yu, S.-H. Jun, J. Choi, M.-H. Kim, Origin of graphite exfoliation an investigation of the important role of solvent cointercalation, J. Electrochem. Soc. 147 (2000) 4391, http://dx.doi.org/10.1149/1.1394076.

[59] J.M. Tarascon, D. Guyomard, New electrolyte compositions stable over the O-V to 5-V voltage range and compatible with the Li1+Xmn2O4 carbon Li-Ion cells, Solid State Ionics 69 (1994) 293–305, http://dx.doi.org/10.1016/0167-2738(94)90418-9.

[60] N. Zhang, H. Tang, Dissecting anode swelling in commercial lithium-ion batteries, J. Power Sources 218 (2012) 52–55, http://dx.doi.org/10.1016/j.jpowsour.2012.06.071.

[61] E.M.C. Jones, Ö.Ö. Çapraz, S.R. White, N.R. Sottos, Reversible and irreversible deformation mechanisms of composite graphite electrodes in lithium-ion batteries, J. Electrochem. Soc. 163 (2016) A1965–A1974, http://dx.doi.org/10.1149/2.0751609jes.

[62] J.B. Siegel, a. G. Stefanopoulou, P. Hagans, Y. Ding, D. Gorsich, Expansion of lithium ion pouch cell batteries: observations from neutron imaging, J. Electrochem. Soc. 160 (2013) A1031–A1038, http://dx.doi.org/10.1149/2.011308jes.

[63] R. Hausbrand, G. Cherkashinin, H. Ehrenberg, M. Gröting, K. Albe, C. Hess, W. Jaegermann, Fundamental degradation mechanisms of layered oxide Li-ion battery cathode materials: methodology, insights and novel approaches, Mat. Sci. Eng. B Solid-State Mat. Adv. Technol. 192 (2015) 3–25, http://dx.doi.org/10.1016/j.mseb.2014.11.014.

[64] B. Rieger, S. Schlueter, S.V. Erhard, J. Schmalz, G. Reinhart, A. Jossen, Multi-scale investigation of thickness changes in a commercial pouch type lithium-ion battery, Adv. Life Course Res. 6 (2016) 213–221, http://dx.doi.org/10.1016/j.est.2016.01.006.

[65] M. Onuki, S. Kinoshita, Y. Sakata, M. Yanagidate, Y. Otake, M. Ue, M. Deguchi, Identification of the source of evolved gas in Li-Ion batteries using 13C-labeled solvents, J. Electrochem. Soc. 155 (2008) A794, http://dx.doi.org/10.1149/1.2969947.

[66] K. Edström, T. Gustafsson, J.O. Thomas, The cathode-electrolyte interface in the Li-ion battery, Electrochim. Acta 50 (2004) 397–403, http://dx.doi.org/10.1016/j.electacta.2004.03.049.

[67] K. Jalkanen, J. Karppinen, L. Skogström, T. Laurila, M. Nisula, K. Vuorilehto, Cycle aging of commercial NMC/graphite pouch cells at different temperatures, Appl. Energy 154 (2015) 160–172, http://dx.doi.org/10.1016/j.apenergy.2015.04.110.

[68] D. Aurbach, Review of selected electrode – solution interactions which determine the performance of Li and Li ion batteries, J. Power Sources 89 (2000) 206–218 https://doi.org/10.1016/S0378-7753(00)00431-6.

[69] Y.-K. Sun, Structural degradation mechanism of oxysulfide spinel LiAl 0.24Mn1.76O3.98S0.02 cathode materials on high temperature cycling, Electrochem. Commun. 3 (2001) 199–202, http://dx.doi.org/10.1016/S1388-2481(01)00141-2.

[70] I. Buchberger, S. Seidlmayer, A. Pokharel, M. Piana, J. Hattendorff, P. Kudejova, R. Gilles, H.A. Gasteiger, Aging analysis of graphite/LiNi 1/3 Mn 1/3 Co 1/3 O 2 cells using XRD, PGAA, and AC impedance, J. Electrochem. Soc. 162 (2015) 2737–2746, http://dx.doi.org/10.1149/2.0721514jes.

[71] R. Younesi, A.S. Christiansen, R. Scipioni, D.-T. Ngo, S.B. Simonsen, K. Edström, J. Hjelm, P. Norby, Analysis of the interphase on carbon black formed in high voltage batteries, J. Electrochem. Soc. 162 (2015) A1289–A1296, http://dx.doi.org/10.1149/2.0761507jes.

[72] S. Watanabe, M. Kinoshita, T. Hosokawa, K. Morigaki, K. Nakura, Capacity fade of LiAlyNi1-x-yCoxO 2 cathode for lithium-ion batteries during accelerated calendar and cycle life tests (surface analysis of LiAlyNi1-x-yCo xO2 cathode after cycle tests in restricted depth of discharge ranges), J. Power Sources 258 (2014) 210–217, http://dx.doi.org/10.1016/j.jpowsour.2014.02.018.

[73] X. Li, M. Xu, Y. Chen, B.L. Lucht, Surface study of electrodes after long-term cycling in Li 1.2Ni0.15Mn0.55Co0.1O 2-graphite lithium-ion cells, J. Power Sources 248 (2014) 1077–1084, http://dx.doi.org/10.1016/j.jpowsour.2013.10.044.

[74] S. Watanabe, M. Kinoshita, K. Nakura, Capacity fade of LiNi(1-x-y)CoxAlyO 2 cathode for lithium-ion batteries during accelerated calendar and cycle life test. I. Comparison analysis between LiNi(1-x-y)Co xAlyO2 and LiCoO2 cathodes in cylindrical lithium-ion cells during long term storage test, J. Power sources. 247 (2014) 412–422, http://dx.doi.org/10.1016/j.jpowsour.2013.08.079.

[75] F. Lin, I.M. Markus, D. Nordlund, T.-C. Weng, M.D. Asta, H.L. Xin, M.M. Doeff, Surface reconstruction and chemical evolution of stoichiometric layered cathode materials for lithium-ion batteries, Nat. Commun. 5 (2014) 3529, http://dx.doi.

org/10.1038/ncomms4529.
[76] J. Li, H. Liu, J. Xia, M. Nie, G. Botton, J.R. Dahn, The impact of electrolyte additives and upper cut-off voltage on the formation of a rocksalt surface layer in LiNi0.8Mn0.1Co0.1 electrodes, J. Electrochem. Soc. 164 (2017) A655, http://dx.doi.org/10.1149/2.0651704jes.
[77] S. Watanabe, M. Kinoshita, T. Hosokawa, K. Morigaki, K. Nakura, Capacity fading of LiAlyNi1-x-yCoxO 2 cathode for lithium-ion batteries during accelerated calendar and cycle life tests (effect of depth of discharge in charge-discharge cycling on the suppression of the micro-crack generation of LiAlyNi 1-x-yCoxO2 parti, J. Power Sources. 260 (2014) 50–56, http://dx.doi.org/10.1016/j.jpowsour.2014.02.103.
[78] J. Syzdek, M. Marcinek, R. Kostecki, Electrochemical activity of carbon blacks in LiPF6-based organic electrolytes, J. Power Sources 245 (2014) 739–744, http://dx.doi.org/10.1016/j.jpowsour.2013.07.033.
[79] R.E. Ruther, A.F. Callender, H. Zhou, S.K. Martha, J. Nanda, Raman microscopy of lithium-manganese-rich transition metal oXide cathodes, J. Electrochem. Soc. 162 (2014) A98–A102, http://dx.doi.org/10.1149/2.0361501jes.